Supplementary Material

Francisco Arca,[1, a)] Juan P. Mendez,[2, b)] Michael Ortiz,[3, c)] and Pilar Ariza[1, d)]

[1)]*Escuela Técnica Superior de Ingeniería, University of Seville, 41092, Seville, Spain*

[2)]*Sandia National Laboratories, Albuquerque, 87123, NM, USA*

[3)]*Division of Engineering and Applied Science, California Institute of Technology, CA, 91125, Pasadena, USA*

[a)]Electronic mail: farca@us.es

[b)]Electronic mail: jpmende@sandia.gov

[c)]Electronic mail: ortiz@caltech.edu

[d)]Electronic mail: mpariza@us.es

SUPPLEMENTARY MATERIAL 1: TWINNING CONFIGURATIONS

Fig. 1 shows the fully-relaxed atomic configuration of the twins (15,8), (19,8), (19,12) and (19,16), as reported in Arca *et al.*[1].

SUPPLEMENTARY MATERIAL 2: TRANSPORT CALCULATION METHODOLOGY

Landauer-Büttiker formalism

For completeness and ease of reference, in this section we briefly summarize the basis of the Landauer-Büttiker formalism (cf. Datta[2,3]). The tight-binding Hamiltonian matrix (TBHM) of the model sketched in Fig. 2 can be written in terms of submatrices as

$$\boldsymbol{H} = \begin{pmatrix} \boldsymbol{H}_L & \boldsymbol{H}_{LC} & \mathbf{0} \\ \boldsymbol{H}_{CL} & \boldsymbol{H}_C & \boldsymbol{H}_{CR} \\ \mathbf{0} & \boldsymbol{H}_{RC} & \boldsymbol{H}_R \end{pmatrix}, \tag{1}$$

where $\boldsymbol{H}_C$ corresponds to the central component, $\boldsymbol{H}_{L(R)}$ corresponds to the isolated semi-infinite left (right) component and $\boldsymbol{H}_{L(R)C}$ represents the coupling between the left (right) and central regions of the model. Within the TB formalism, the empirical TBHM follows as

$$H_{l\alpha,j\beta} = E_\alpha \delta_{lj}\delta_{\alpha\beta} + h_{l\alpha,j\beta}(1-\delta_{lj}\delta_{\alpha\beta}), \tag{2}$$

where l and j label atomic sites, α and β label atomic orbitals, and E_α and $h_{l\alpha,j\beta}$ are the on-site parameters and hopping functions, respectively.

Bloch's theorem is applicable to periodic systems such as those considered in this work[4]. In $\boldsymbol{k}$-space, the sizes of the submatrices $\boldsymbol{H}_C(\boldsymbol{k})$, $\boldsymbol{H}_{L(R)}(\boldsymbol{k})$ and $\boldsymbol{H}_{L(R)C}(\boldsymbol{k})$ are $[N_c \times N_c]$, $[\infty \times \infty]$ and $[\infty \times N_c]$, respectively, where N_c is the number of atoms in the central region.

Following Datta[2,3], the transmission function T across the central region at energy E can be written in the form

$$T(E) = \frac{1}{N}\sum_{\boldsymbol{k}}^{N} Tr[\boldsymbol{\Gamma}_L(E,\boldsymbol{k})\boldsymbol{G}_C^{\dagger}(E,\boldsymbol{k})\boldsymbol{\Gamma}_R(E,\boldsymbol{k})\boldsymbol{G}_C(E,\boldsymbol{k})], \tag{3}$$

where $\boldsymbol{\Gamma}_L(E,\boldsymbol{k})$ and $\boldsymbol{\Gamma}_R(E,\boldsymbol{k})$ are the coupling $[N_c \times N_c]$ matrices, accounting for the coupling between the central and the left (right) regions, and $\boldsymbol{G}_C$ is Green's matrix of the central region. We recall that the transmission function provides the rate at which electrons are transmitted across the

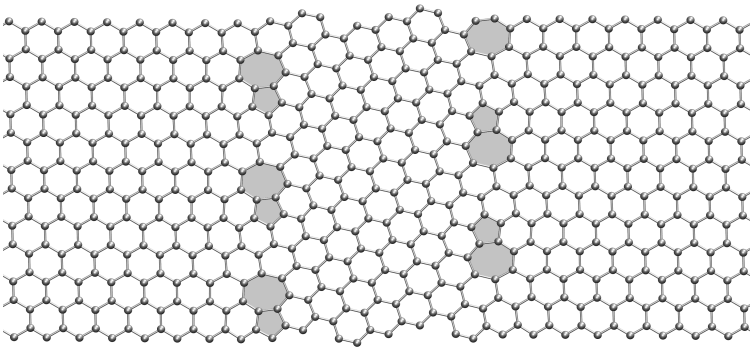

(a)

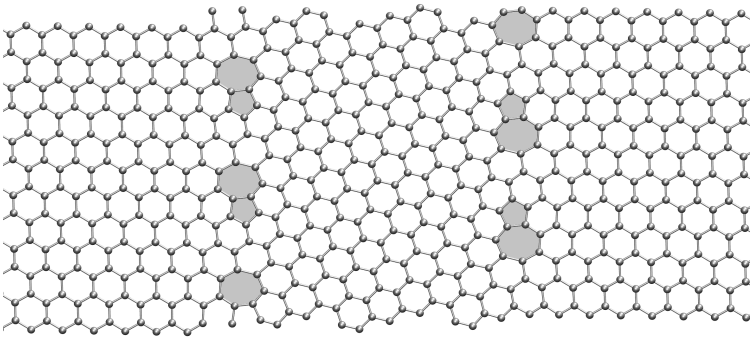

(b)

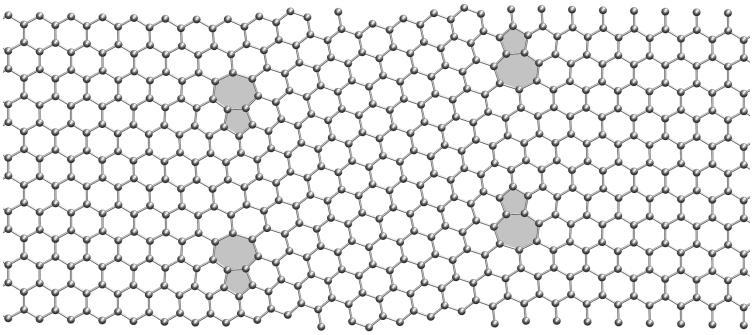

(c)

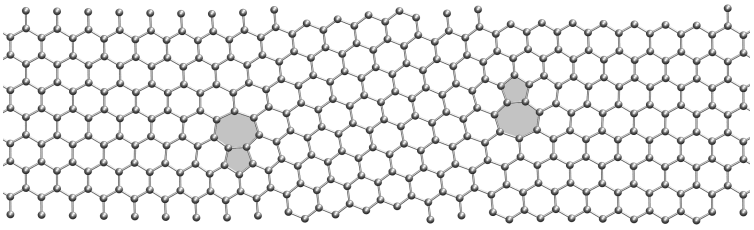

(d)

FIG. 1: Relaxed atomic configurations of the dislocation structures considered in this work: (a) (15,8), (b) (19,8), (c) (19,12), and (d) (19,16).

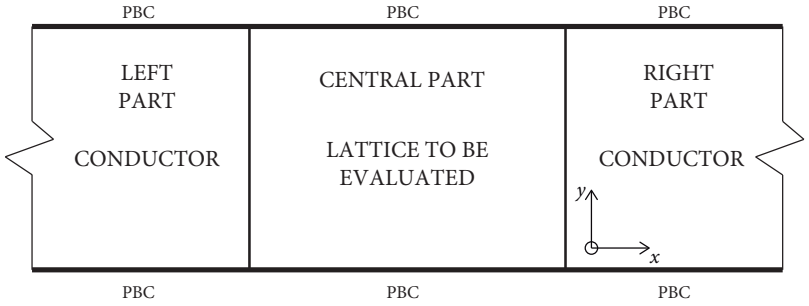

FIG. 2: Geometry of the model used to compute charge carrier transmission across a lattice.

central region. For economy of notation, henceforth we drop the $\boldsymbol{k}$-dependence of the submatrices. The central region Green's matrix, $\boldsymbol{G}_C$, follows readily as

$$\boldsymbol{G}_C(E) = [E^+\mathbb{I} - \boldsymbol{H}_C - \boldsymbol{\Sigma}_L(E) - \boldsymbol{\Sigma}_R(E)]^{-1} \approx [E\mathbb{I} - \boldsymbol{H}_C - \boldsymbol{\Sigma}_L(E) - \boldsymbol{\Sigma}_R(E)]^{-1}, \tag{4}$$

where $E^+ = E + i\eta$, with $\eta \to 0^+$, $\boldsymbol{\Sigma}_L$ and $\boldsymbol{\Sigma}_R$ are the self-energy $[N_c \times N_c]$ matrices corresponding to the left and right regions, respectively, which describe the effect of these regions on the electronic structure of the central region. We have,

$$\boldsymbol{\Sigma}_l(E) = \boldsymbol{H}_{Cl}\boldsymbol{G}_l(E)\boldsymbol{H}_{lC}, \quad l = L,R, \tag{5}$$

where

$$\boldsymbol{G}_l(E) = (E^+\mathbb{I} - \boldsymbol{H}_l)^{-1}, \quad l = L,R \tag{6}$$

are the semi-infinite left and right regions Green's functions, respectively. It can be shown that the self-energy matrices, $\boldsymbol{\Sigma}_L(E)$ and $\boldsymbol{\Sigma}_R(E)$, can be further reduced to

$$\boldsymbol{\Sigma}_l(E) = \boldsymbol{H}_{Cl}\boldsymbol{G}_l^0(E)\boldsymbol{H}_{lC}, \quad l = L,R, \tag{7}$$

where $\boldsymbol{G}_L^0(E)$ and $\boldsymbol{G}_R^0(E)$ are the surface Green's matrices of the left and right regions, respectively. In order to compute these matrices, we follow the recursive method of Li and Lu[5], John and Pulfrey[6] and Sancho *et al.*[7]. Finally, the coupling matrices follow as

$$\boldsymbol{\Gamma}_l(E) = \imath(\boldsymbol{\Sigma}_l(E) - \boldsymbol{\Sigma}_l^\dagger(E)), \quad l = L,R \tag{8}$$

i. e., as the difference between the retarded and the advanced self-energy matrices.

Tight-binding model

The TBH matrix has the structure

$$\begin{array}{c} \\ 1 \\ \vdots \\ i \\ \vdots \\ N \end{array} \begin{array}{c} \begin{array}{ccccc} 1 & \dots & j & \dots & N \end{array} \\ \begin{pmatrix} \boldsymbol{H}_{1\alpha,1\beta} & \dots & \dots & \dots & \boldsymbol{H}_{1\alpha,N\beta} \\ \vdots & \vdots & \vdots & \vdots & \vdots \\ \dots & \dots & \boldsymbol{H}_{i\alpha,j\beta} & \dots & \dots \\ \vdots & \vdots & \vdots & \vdots & \vdots \\ \boldsymbol{H}_{N\alpha,1\beta} & \dots & \dots & \dots & \boldsymbol{H}_{N\alpha,N\beta} \end{pmatrix} \end{array}. \tag{9}$$

When $i \neq j$, the sub-matrices are called hopping sub-matrices and have the form

$$\boldsymbol{H}_{i\alpha,j\beta} = \begin{pmatrix} h_{is,js} & h_{is,jp_x} & h_{is,jp_y} & h_{is,jpz} \\ h_{ip_x,js} & h_{ip_x,jp_x} & h_{ip_x,jp_y} & h_{ip_x,jp_y} \\ h_{ip_y,js} & h_{ip_y,jp_x} & h_{ip_y,jp_y} & h_{ip_y,jp_z} \\ h_{ip_z,js} & h_{ip_z,jp_x} & h_{ip_z,jp_y} & h_{ip_z,jp_z} \end{pmatrix} =$$

$$\begin{pmatrix} h_{ss\sigma} & d_x h_{sp\sigma} & d_y h_{sp\sigma} & d_z h_{sp\sigma} \\ -d_x h_{sp\sigma} & d_x^2 h_{pp\sigma} + d_y^2 h_{pp\pi} & d_x d_y (h_{pp\sigma} - h_{pp\pi}) & d_x d_z (h_{pp\sigma} - h_{pp\pi}) \\ -d_y h_{sp\sigma} & d_x d_y (h_{pp\sigma} - h_{pp\pi}) & d_x^2 h_{pp\sigma} + (1 - d_y^2) h_{pp\pi} & d_y d_z (h_{pp\sigma} - h_{pp\pi}) \\ -d_z h_{sp\sigma} & d_z d_x (h_{pp\sigma} - h_{pp\pi}) & d_z d_y (h_{pp\sigma} - h_{pp\pi}) & d_z^2 h_{pp\sigma} + (1 - d_z^2) h_{pp\pi} \end{pmatrix}, \tag{10}$$

where $h_{ss\sigma}$, $h_{sp\sigma}$, $h_{pp\sigma}$ and $h_{pp\pi}$ are the hopping parameters between atoms i and j, and d_x, d_y and d_z are the directional cosines defined as

$$d_x = \frac{\boldsymbol{r}_{ij} \cdot \boldsymbol{x}}{r_{ij}}, \tag{11}$$

$$d_y = \frac{\boldsymbol{r}_{ij} \cdot \boldsymbol{y}}{r_{ij}}, \tag{12}$$

$$d_z = \frac{\boldsymbol{r}_{ij} \cdot \boldsymbol{z}}{r_{ij}}, \tag{13}$$

where $\boldsymbol{x}$, $\boldsymbol{y}$ and $\boldsymbol{z}$ represent the unit vectors of a cartesian coordinate system

$$\boldsymbol{x} = \begin{pmatrix} 1 \\ 0 \\ 0 \end{pmatrix}, \quad \boldsymbol{y} = \begin{pmatrix} 0 \\ 1 \\ 0 \end{pmatrix}, \quad \boldsymbol{z} = \begin{pmatrix} 0 \\ 0 \\ 1 \end{pmatrix}, \tag{14}$$

and $\boldsymbol{r}_{ij}$ is the vector that goes from atom i to atom j, and r_{ij} is the norm of the vector. Normally, $h_{ss\sigma}$, $h_{sp\sigma}$, $h_{pp\sigma}$ and $h_{pp\pi}$ are functions of the interatomic distance between atoms i and j.

When $i = j$, the sub-matrices are called on-site sub-matrices and have the form

$$\boldsymbol{H}_{ii} = \begin{pmatrix} h_{is,is} & 0 & 0 & 0 \\ 0 & h_{ip_x,ip_x} & 0 & 0 \\ 0 & 0 & h_{ip_y,ip_y} & 0 \\ 0 & 0 & 0 & h_{ip_z,ip_z} \end{pmatrix} = \begin{pmatrix} E_s & 0 & 0 & 0 \\ 0 & E_{p_x} & 0 & 0 \\ 0 & 0 & E_{p_y} & 0 \\ 0 & 0 & 0 & E_{p_z} \end{pmatrix}. \tag{15}$$

Definition of the tight binding Hamiltonian matrix in k-space

The Hamiltonian matrix in k-space for pristine graphene lattice is defined by the sub-matrices

$$\hat{\boldsymbol{H}} = \begin{pmatrix} \hat{\boldsymbol{H}}\binom{\boldsymbol{k}}{11} & \hat{\boldsymbol{H}}\binom{\boldsymbol{k}}{12} \\ \hat{\boldsymbol{H}}\binom{\boldsymbol{k}}{21} & \hat{\boldsymbol{H}}\binom{\boldsymbol{k}}{22} \end{pmatrix}. \tag{16}$$

Since the unit cell is composed of two atoms, labeled as atom type 1 and 2 in our model, the TBH matrix is built from 4 sub-matrices.

Taking into account interactions up to the first-nearest neighbors for the hopping parameters, we have

$$\hat{\boldsymbol{H}}\begin{pmatrix} \boldsymbol{k} \\ 11 \end{pmatrix} = \hat{\boldsymbol{H}}\begin{pmatrix} \boldsymbol{k} \\ 22 \end{pmatrix} = \begin{pmatrix} E_s & 0 & 0 & 0 \\ 0 & E_p & 0 & 0 \\ 0 & 0 & E_p & 0 \\ 0 & 0 & 0 & E_p \end{pmatrix}, \tag{17}$$

$$\hat{H}\begin{pmatrix} \boldsymbol{k} \\ 12 \end{pmatrix} = \sum_j e^{\imath \boldsymbol{k}\cdot\boldsymbol{r}_{ij}}.$$

$$\begin{pmatrix} h_{ss\sigma} & d_x \cdot h_{sp\sigma} & d_y \cdot h_{sp\sigma} & d_z \cdot h_{sp\sigma} \\ -d_x \cdot h_{sp\sigma} & d_x^2 \cdot h_{pp\sigma} + d_y^2 \cdot h_{pp\pi} & d_x \cdot d_y \cdot (h_{pp\sigma} - h_{pp\pi}) & d_x \cdot d_z \cdot (h_{pp\sigma} - h_{pp\pi}) \\ -d_y \cdot h_{sp\sigma} & d_x \cdot d_y \cdot (h_{pp\sigma} - h_{pp\pi}) & d_x^2 \cdot h_{pp\sigma} + (1 - d_y^2) \cdot h_{pp\pi} & d_y \cdot d_z \cdot (h_{pp\sigma} - h_{pp\pi}) \\ -d_z \cdot h_{sp\sigma} & d_z \cdot d_x \cdot (h_{pp\sigma} - h_{pp\pi}) & d_z \cdot d_y \cdot (h_{pp\sigma} - h_{pp\pi}) & d_z^2 \cdot h_{pp\sigma} + (1 - d_z^2) \cdot h_{pp\pi} \end{pmatrix}, \tag{18}$$

$$\hat{H}\begin{pmatrix} \boldsymbol{k} \\ 21 \end{pmatrix} = \hat{H}^{\dagger}\begin{pmatrix} \boldsymbol{k} \\ 12 \end{pmatrix}, \tag{19}$$

where j runs over the first-nearest neighbors of atom i.

SUPPLEMENTARY MATERIAL 3: VALIDATION OF THE DEFORMATION

For verification purposes, we have also computed the deformed configuration of the dislocation structures $(15,8)$ using the DFT SIESTA code[8]. Fig. 3 shows the resulting structure for $\varepsilon_x = 0.18$

using molecular dynamics (MD) and the AIREBO potential, and DFT-based MD calculations. As is evident from the figure, in general both configurations show good agreement for the atomic structure, although we observe small discrepancies in the y-dimension of the cell due to the difference in the lattice constant predicted by AIREBO, 1.397 Å, and SIESTA, 1.42 Å.

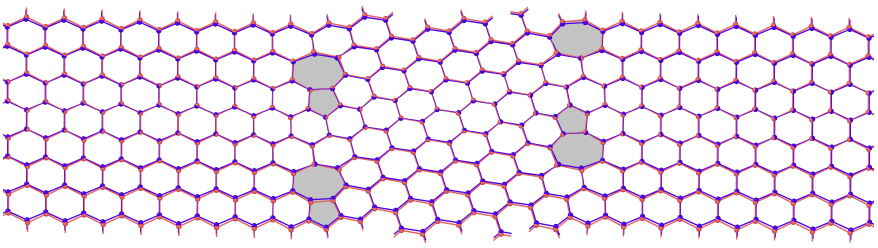

FIG. 3: Comparison of the (15,8) configuration under a uniaxial strain of $\varepsilon_x = 0.18$, calculated with LAMMPS-AIREBO (blue) and with SIESTA (red).

This calculation was carried out employing the PBE exchange–correlation functional within the generalized gradient approximation (GGA)[9], the double-ξ with polarization basis set[10], and smooth norm-conserving pseudopotentials[11]. We apply an increasing force in the x-direction until the target deformation is reached and conjugate gradients (CG) energy-minimization in every step to obtain the equilibrium structure. We use a grid of 80 k-points and a mesh cut-off of 300 Ry.

SUPPLEMENTARY REFERENCES

[1]F. Arca, J. P. Mendez, M. Ortiz, and M. P. Ariza, "Spontaneous twinning as an accommodation mechanism in monolayer graphene," European Journal of Mechanics - A/Solids **80**, 103923 (2020).

[2]S. Datta, *Electronic Transport in Mesoscopic Systems* (Cambridge University Press, Cambridge, 1995).

[3]S. Datta, *Quantum transport: Atom to Transistor* (Cambridge University Press, Cambridge, 2005).

[4]C. Kittel, *Introduction to Solid State Physics*, 8th ed. (John Wiley & Sons, Inc., New York, 2004).

[5]T. C. Li and S.-P. Lu, "Quantum conductance of graphene nanoribbons with edge defects," Phys. Rev. B **77**, 085408 (2008).

[6]D. L. John and D. L. Pulfrey, "Green's function calculations for semi-infinite carbon nanotubes," physica status solidi (b) **243**, 442–448 (2006).

[7]M. P. L. Sancho, J. M. L. Sancho, J. M. L. Sancho, and J. Rubio, "Highly convergent schemes for the calculation of bulk and surface green functions," Journal of Physics F: Metal Physics **15**, 851 (1985).

[8]J. M. Soler, E. Artacho, J. D. Gale, A. García, J. Junquera, P. Ordejón, and D. Sánchez-Portal, "The siesta method for ab initio order-n materials simulation," Journal of Physics: Condensed Matter **14**, 2745 (2002).

[9]J. Perdew, K. Burke, and M. Ernzerhof, "Generalized gradient approximation made simple," Phys. Rev. Lett. **77**, 3865–3868 (1996).

[10]J. Junquera, O. Paz, D. Sańchez-Portal, and E. Artacho, "Numerical atomic orbitals for linear-scaling calculations," Physical Review B **64** (2001).

[11]N. Troullier and J. Martins, "Efficient pseudopotentials for plane-wave calculations," Phys. Rev. B **43**, 1993–2006 (1991).